https://doi.org/10.5194/essd-2023-411
Preprint. Discussion started: 11 December 2023

Open Access Earth System Science Data Discussions

A Frontal Ablation Dataset for 49 Tidewater Glaciers in Greenland

Dominik Fahrner[1], Donald Slater[2], Aman KC[3], Claudia Cenedese[4], David A. Sutherland[1], Ellyn Enderlin[3], Femke de Jong[5], Kristian K. Kjeldsen[6], Michael Wood[7,8], Peter Nienow[2], Sophie Nowicki[9], Till Wagner[10]

[1] University of Oregon, Department of Earth Sciences, USA
[2] University of Edinburgh, School of Geosciences, UK
[3] Boise State University, Department of Geosciences, USA
[4] Woods Hole Oceanographic Institution, Physical Oceanography Department, USA
[5] Royal Netherlands Institute for Sea Research, the Netherlands
[6] Geological Survey of Denmark and Greenland, Denmark
[7] Moss Landing Marine Laboratories, San José State University, USA
[8] Jet Propulsion Laboratory, California Institute of Technology, USA
[9] University at Buffalo, Department of Geology, USA
[10] University of Wisconsin-Madison, Department of Atmospheric and Oceanic Sciences, USA

Correspondence to: Dominik Fahrner (dfahrner@uoregon.edu)

Abstract

Frontal ablation at tidewater glaciers, which comprises iceberg calving, submarine and subaerial melting, is a key boundary condition for numerical ice sheet models but remains difficult to measure directly in-situ. Many previous studies have quantified frontal ablation over varying spatio-temporal scales, however most use ice discharge as an approximation for frontal ablation, thereby neglecting the influence of terminus location change. Frontal ablation estimates that do account for terminus location change are spatio-temporally limited by the availability of observational data. Here, we present a processing chain to quantify frontal ablation using open-source observational data. We apply the processing chain to 49 tidewater glaciers in Greenland with reliable near-terminus bathymetry data in the BedMachine V4 dataset. Near-terminus volume change over the time period 1987 - 2020 is determined using a previously published dataset of terminus positions (TermPicks), ice thicknesses from ArcticDEM and AeroDEM, adjusted for surface elevation change over time, and bathymetry data from BedMachine v4. Assuming a vertical terminus geometry and uniform ice density, we estimate frontal ablation as the difference between mass flux towards the terminus (Mankoff et al., 2020) and mass change between consecutive observation. The frontal ablation dataset offers exciting opportunities for developing

https://doi.org/10.5194/essd-2023-411
Preprint. Discussion started: 11 December 2023

new insights into ice dynamics, including helping to improve numerical model hindcasting and projections. Lastly, we provide a processing chain that may serve as a community standard for determining frontal ablation from observational data for any tidewater glacier.

Introduction

Greenland's tidewater glaciers have been accelerating and retreating since the mid-1990's and contribute ~30-60 % of the total annual mass loss from the Greenland Ice Sheet (GrIS) through frontal ablation (Enderlin et al., 2014; Mouginot et al., 2019; Shepherd et al., 2020). Frontal ablation, which comprises iceberg calving, submarine melting and subaerial melting at the glacier terminus, can be an important component of glacier mass balance and is susceptible to changes over a wide range of time scales (e.g., through changes in ice flow, ocean or air temperatures, or near terminus sea-ice or mélange conditions; e.g. Cowton et al., 2018; King et al., 2020). The volume flux of ice across a fixed gate (referred to as discharge) is often used to approximate frontal ablation, which does not take terminus position change into account (Rignot and Kanagaratnam, 2006).

Studies that do determine frontal ablation while taking terminus position change into account have been conducted over varying spatio-temporal scales (Osmanoğlu et al., 2013; McNabb et al., 2015; Fried et al., 2018; Wagner et al., 2019; Kochtitzky et al., 2022, 2023) and using a variety of data (Köhler et al., 2016; Wychen et al., 2020; Bunce et al., 2021). However, in situ observational data, especially for the GrIS, are often lacking and satellite remote sensing data are temporally limited by image availability. Multi-decadal estimates of frontal ablation are therefore often confined to specific locations (e.g. McNabb et al., 2015) or limited time periods (e.g. Köhler et al., 2016; Bunce et al., 2021). The most recent comprehensive study by Kochtitzky et al. (2023) determined frontal ablation for all glaciers of the GrIS, however their study is constrained to the use of decadal averages.

https://doi.org/10.5194/essd-2023-411
Preprint. Discussion started: 11 December 2023

Open Access Earth System Science Data Discussions

In current, large-scale, numerical ice sheet models, frontal ablation is heavily parameterized and remains a key uncertainty for projecting future sea level rise (Luckman et al., 2015; Benn et al., 2017; Slater et al., 2019; Goelzer et al., 2020). The limited understanding of frontal ablation processes, partially due to the scarcity of observational data, and the lack of long timeseries of frontal ablation further complicate the inclusion of ice-sheet-ocean processes in numerical models (Cowton et al., 2018; Slater et al., 2019). Quantifying frontal ablation from observational data is therefore crucial to improve our understanding of near-terminus ice dynamics and improving numerical modelling efforts (Benn et al., 2017; Cowton et al., 2018)

The processing chain presented here derives multi-decadal time series of frontal ablation for tidewater glaciers located along the Greenland coast using publicly available remote sensing observational data. The high spatio-temporal resolution (up to monthly) of the resulting timeseries can provide new insights into mass loss from tidewater glaciers in Greenland and is aimed at improving the current understanding of ocean forcing of the GrIS.

Product description

At any tidewater glacier, there is a competition of processes that determine whether termini advance, retreat or remain stable. The ice velocity at the terminus pushes the terminus forwards, while calving and melting of subaerial portions of the ice face move the terminus backwards (i.e., in the direction opposite to ice flow). This may be expressed mathematically as

$$\int_A \frac{dL}{dt} dA = \int_A v dA - \int_A (c + m_s + m_a)\, dA \quad (1)$$

in which L is terminus position, v is ice velocity at the terminus, c is calving rate, m_s is submarine melt rate and m_a is subaerial melt rate. Each of these quantities may vary with depth or width along the calving front but in Eq. 1 we integrate over the terminus frontal area A. Note that we define $\frac{dL}{dt}$ as positive for glacier advance and negative for glacier retreat. We

https://doi.org/10.5194/essd-2023-411
Preprint. Discussion started: 11 December 2023

define frontal ablation, F, as the sum of calving, submarine melting, and subaerial melting rates; that is all the processes that remove ice from the calving front.

$$F = \rho_i \int_A (c + m_s + m_a)\, dA \tag{2}$$

where the ice density ρ_i is included so that F is a mass flux. Quantifying frontal ablation directly by estimating calving rate, submarine melt rate and subaerial melt rate is very difficult and uncertain, but we can note from Eq. 1 that

$$F = \rho_i \int_A v\, dA - \rho_i \int_A \frac{dL}{dt}\, dA, \tag{3}$$

which expresses frontal ablation in terms of frontal ice velocity and terminus position change. If we assume that these are relatively depth-invariant (i.e., vertical terminus face and plug flow of ice), then Eq. 3 can be rewritten as

$$F = \rho_i \int_W H v_s dW - \rho_i \int_W H \frac{dL_s}{dt} dW \tag{4}$$

where H is ice thickness, *W* the width of the glacier, and v_s and L_s are the velocity and terminus position at the glacier surface, estimated from readily available remote sensing datasets. Hence, Eq. 4 provides a practical means of estimating frontal ablation. Note that the first term on the right-hand side of Eq. 4 is commonly referred to as the solid ice discharge *D* (e.g. Mankoff et al., 2020) so that frontal ablation differs from solid ice discharge by the mass change relating to terminus position change (hereafter referred to as *TMC*). We therefore simplify Eq. 4 to

$$F = D - TMC. \tag{5}$$

The data product presented here provides frontal ablation estimates for 49 selected tidewater glaciers in Greenland using available terminus position observations from the TermPicks dataset (Goliber and Black, 2021).

The tidewater glaciers included in the dataset were selected based on the reliability of methods that were used to determine fjord bathymetry (Figure 1; Morlighem et al., 2017, 2021; Wood et al., 2021). We include only glaciers where bathymetry data were derived from measurements, mass conservation or the GIMP DEM (as classified in the BedMachine v4

https://doi.org/10.5194/essd-2023-411
Preprint. Discussion started: 11 December 2023

dataset), thereby excluding glaciers where bathymetry was derived synthetically or by interpolation, kriging, or gravity inversion (Morlighem et al., 2017, 2021). However, the presented workflow can be applied to any glacier, independent of the reliability of bathymetry data, provided that the data outlined in the *Data Sources section* are available.

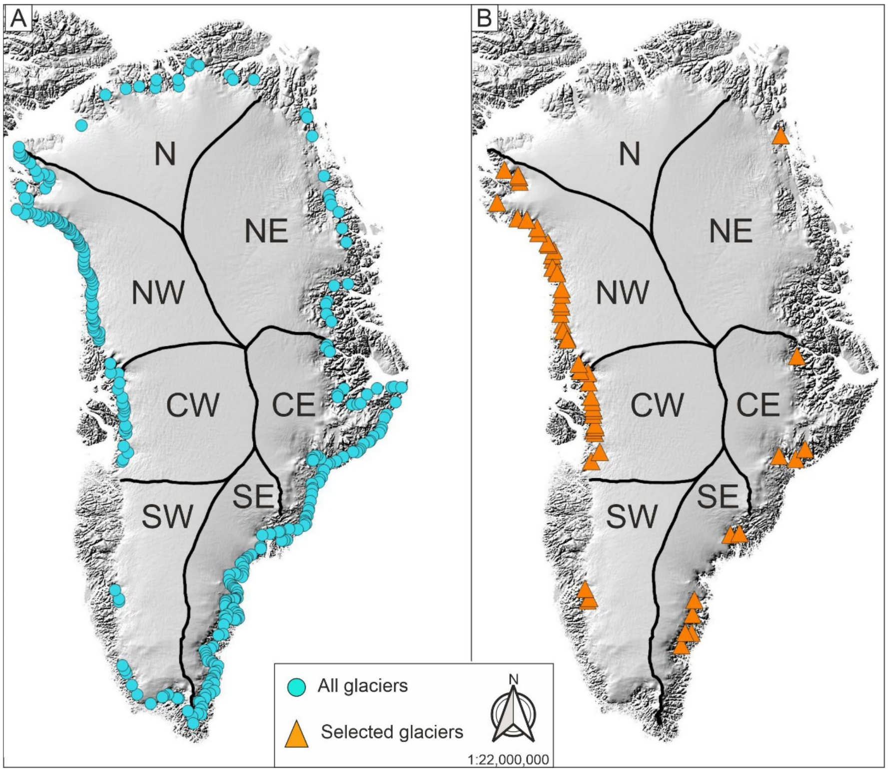

Figure 1 | Overview of Selected tidewater glaciers

A) Location of all tidewater glaciers for which terminus observations are available in the TermPicks dataset (Goliber and Black, 2021). B) Location of tidewater glaciers that have been selected for this study based on the reliability of bathymetry data. The basemap is taken from BedMachine v4 (Morlighem et al., 2017, 2021); lines show drainage basins after Mouginot and Rignot (2019).

https://doi.org/10.5194/essd-2023-411
Preprint. Discussion started: 11 December 2023

Data sources

This section introduces previously published data sources, which are publicly available and were used to calculate frontal ablation. The spatio-temporal resolution of each input dataset as well as the associated uncertainties can be found in Tables S1 and S2.

Terminus positions

We use terminus position data from the TermPicks dataset (Goliber and Black, 2021), which includes manually as well as automatically delineated terminus positions from various sources for the period 1916 to 2020. The availability of terminus delineations varies over time as satellite imagery prior to the start of NASA's Landsat program in 1972 is sparse. The TermPicks dataset and its metadata are considered standardized. However, due to the different sources of the individual terminus delineations, additional filtering is required before they can be used to quantify terminus change over time (see Methods).

Surface elevation, bathymetry, and ice thickness

We use glacier specific surface elevation change rates determined by Khan (2017) for the period 1995 – 2015. These are combined with the latest ArcticDEM image that covers the full extent of the tidewater glacier at its most advanced and most retreated position (Porter et al., 2018) and AeroDEM, which has been derived from stereophotogrammetric imagery recorded during 1978-87 (Korsgaard et al., 2016b). Bedrock topography is taken from BedMachine v4 (Morlighem et al., 2017, 2021). Time series of ice thickness are computed using the DEMs, adjusted to account for surface elevation change, and bedrock topography (see Methods).

Ice Velocity

Ice velocities are taken from NASA's Making Earth System Data Records for Use in Research Environments (MEaSUREs) Inter-Mission Time Series of Land Ice Velocity and Elevation (ITS_LIVE) project. We use composite images, which provide annual flow velocities for the period 1985 – 2018 (Gardner et al., 2019).

https://doi.org/10.5194/essd-2023-411
Preprint. Discussion started: 11 December 2023

Discharge

Solid ice discharge data with uncertainties is taken from Mankoff et al. (2020) for the period 1986 – 2020 and is used to calculate frontal ablation as shown in Eq.5. The flux gates used to derive solid ice discharge are located approximately 5 km upstream of the terminus, so that there could be a time lag and/or difference between the solid ice discharge estimated at the flux gate the discharge at the terminus. Mankoff et al. (2020) estimate the difference in discharge between gates located 1 km and 5 km from the terminus to be around 5% at the ice sheet scale, but it is unclear how much of this difference arises due to uncertainty in bed topography, which generally increases closer to the terminus. Acknowledging this small possible difference, together with the strong longitudinal stress coupling at fast-flowing tidewater glaciers (e.g. Enderlin et al., 2016), we here take the discharge from the flux gates 5 km upstream to be representative of the flux at the terminus. Following Mankoff et al. (2020), we also assign an error of ~10% to these discharge values (see later).

Satellite Imagery

NASA Landsat 8 satellite imagery are downloaded from NASA's Earth Explorer for each individual glacier, and true-color, panchromatically sharpened images are created using the red, blue, green, and panchromatic band (Bands 2, 3, 4 and 8). The pan-sharpened true-color images are used to manually digitize fjord walls, which are used to bring terminus delineations to a consistent length and to create polygons for each observation.

Methods

Fjord geometry

Tidewater glacier terminus positions in the TermPicks dataset vary widely in their length and differ in their starting/end points. For example, traces for an individual glacier could be drawn in opposing directions (e.g., from North to South as well as South to North), which will be referred to as drawing direction hereafter, depending on the author. This variability in terminus trace drawing direction therefore necessitates standardization for further processing.

https://doi.org/10.5194/essd-2023-411
Preprint. Discussion started: 11 December 2023

Here fjord boundaries are created by manually delineating the upper and lower fjord walls using pansharpened NASA Landsat 8 imagery, with the coordinates of the boundaries being saved so that this step only has to be completed once. Subsequently, the drawing direction is standardized based on the distance between the terminus delineation endpoint and the fjord walls. If the end point of the terminus delineation is located closer to the lower fjord wall than the upper fjord wall the terminus delineation is rotated (Figure 2).

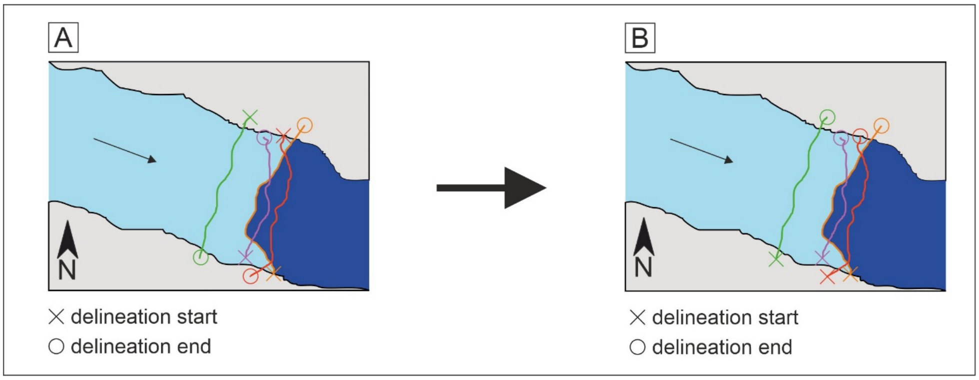

Figure 2 | Sketch of drawing direction

A) Example of drawing directions of terminus delineations in TermPicks dataset, with termini start and endpoints (indicated by *x* and *o* symbols respectively) indicating if they have been traced North to South or South to North. B) Terminus delineations after standardizing drawing directions for further processing.

Definition of upstream boundary

A reference boundary needs to be defined so that individual terminus positions can be compared to each other. This boundary is defined manually by drawing an arbitrary line upstream of the most retreated position of the glacier that intersects both fjord walls on top of a pansharpened true color NASA Landsat 8 image. The reference boundary is fixed and remains the same for all terminus positions at a given glacier over time.

Polygons are created for each terminus observation by combining the reference boundary, respective terminus delineation and the fjord wall boundaries between these two locations. The polygons, herein referred to as the area of interest (AOI), provide the basis for the calculation of area and volume change between observations.

https://doi.org/10.5194/essd-2023-411
Preprint. Discussion started: 11 December 2023

Terminus positions

The TermPicks delineations of all investigated tidewater glaciers are first visually examined to identify obvious outliers caused by e.g., false georeferencing of the satellite image or delineation of mélange. We then subsampled the TermPicks dataset (Goliber and Black, 2021) by using approximately monthly terminus traces selected as the closest in time to the 1st of the month in each month. We also restricted the terminus positions to lie within the period of ice discharge estimates (1986-present; Mankoff et al., 2020). While this reduces the amount of terminus position observations, at times drastically, we found that the uncertainties associated with delineations created by different authors are too high to ensure an accurate product at higher temporal resolution. We chose delineations based on their time difference to the 1st day of the respective month to enable subsequent temporal averaging.

In a second step, the monthly terminus observations are filtered to remove erroneous delineations (e.g., due to false geolocation of the underlying satellite image) and to ensure consistency in the dataset. The filtering is conducted in multiple, sequential steps, as follows:

1) Terminus delineations are removed if they contain more than one line segment, which can occur, for example, if the terminus is split by a nunatak and the terminus has been delineated in two parts. While it would be possible to linearly interpolate between the line segments, this would skew the data and introduce unnecessary errors when combined with fully-delineated termini.
2) Delineations which are smaller than 95 % of the terminus width, which is defined as the minimum distance between the two fjord walls, are excluded from further analysis. We further exclude terminus positions that are longer than the mean fjord width plus two standard deviations of the mean terminus length, as theses delineations would skew the subsequent mass change calculations (Figure 3). This filtering step ensures that the delineations used for further analysis represent the glacier terminus accurately.

https://doi.org/10.5194/essd-2023-411
Preprint. Discussion started: 11 December 2023

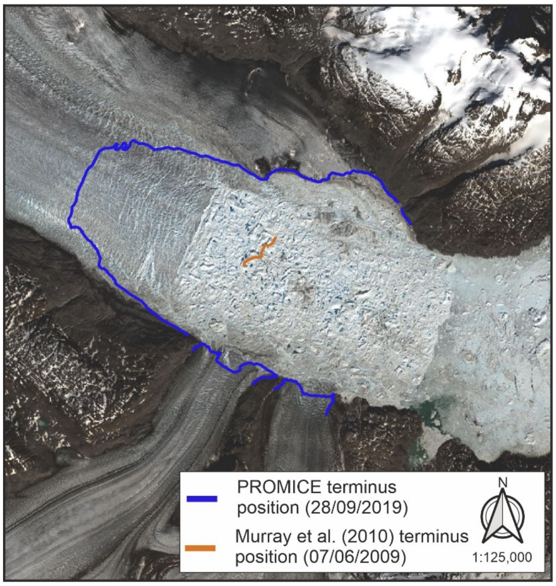

Figure 3 | Example of unusable delineations

The figure shows a terminus delineation from 28/9/2019 by PROMICE (blue) and from Murray et al. (2010) from 07/06/2009 (orange) for Kangerlussuaq Glacier on top of a panchromatic RGB (band-stacked) NASA Landsat 8 image from 30/6/2021. These delineations are examples of unusable terminus traces as they are significantly shorter than the actual terminus width (Murray et al., 2015) or include delineations of the fjord walls (PROMICE).

3) We use NASA MEaSUREs ice velocity to filter out terminus traces that indicate the front has advanced faster than the ice velocity, which is physically not possible. The annual composite velocity images are automatically downloaded when first running the code (Greene et al., 2017). Ice flow velocities are subsequently extracted along a centerline between the most retreated and most advanced terminus position for each glacier. This method is chosen to ensure that velocities are representative of the terminus region and are not skewed by slower flowing parts of the glacier (e.g., lateral drag at the margins). The flow velocities are then averaged for the decade preceding the last available velocity observation to create a decadal mean value velocity.

   Terminus advance is determined using the normal *n* to the connection of midpoints (m_1 and m_2) of subsequent delineations (t_1 and t_2; Figure 4). If the midpoint of the subsequent delineation is located down-fjord of the normal, the glacier movement is classified as advance. Terminus advance or retreat is quantified by calculating the distance between delineation midpoints along a centerline. Then, to ensure that the delineations represent realistic changes in terminus positions, we use the decadal mean near-terminus velocity to infer how much the glacier could have advanced during

https://doi.org/10.5194/essd-2023-411
Preprint. Discussion started: 11 December 2023

each terminus observation timestep. If the terminus advance is greater than twice the predicted flow velocity, the terminus delineation is considered erroneous and is excluded from the dataset.

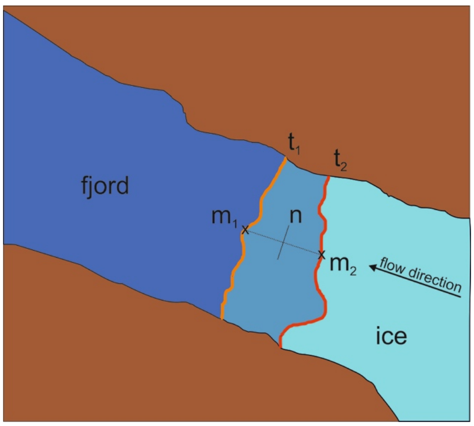

Figure 4 | Sketch of glacier advance/retreat determination for filtering

The normal (n) to the line connecting the midpoints (m_1 and m_2) of subsequent terminus delineations (t_1 and t_2) is used to determine advance and retreat of the glacier. In the sketch shown here, m_2 is right of the normal n, therefore the glacier has retreated. The classification of advance/retreat is solely used for filtering purposes.

During this phase we further exclude the originally selected glaciers Kjer and Nordenskiöld from the analysis as the fjord walls are extremely difficult to delineate, as well as Zachariae Isstrøm and Qeqertaarsuusarsuup Sermia due to their floating ice shelves to reach the final 49 selected systems. The manual delineation of ice shelves is challenging due to their complex structure and the difficulty of distinguishing between terminus and mélange. It should be noted that input terminus delineations should be as accurate as possible to avoid large uncertainties in the frontal ablation estimates. Overall, after quality control and temporal filtering, the dataset contains 34.9 % of all terminus delineations (6674 of 19120; Table S1) for the selected 49 glaciers. An overview of the number of terminus positions pre- and post-filtering can be found in Figure S1. The filtered dataset is the basis of all further analysis and is written to individual shapefiles for manual quality control and to speed up future processing.

Subsequently, in order to accurately compute terminus area change using the filtered time series, the length of each terminus position must be set to be consistent with the previously defined fjord wall boundaries. To determine the location of the start/end points in relation to the fjord walls, the fjord wall polylines are converted into a polygon. If the start/end point lies within the respective boundary polygon, the terminus delineation is clipped, and the new start/endpoint is defined as the intersection point between terminus delineation and boundary polygon (Figure 5 A, B). If the point lies outside of the boundary polygon, the terminus delineation is extrapolated to the nearest point on the boundary polygon (Figure 5 C, D). We compare the length of the extrapolation to the length of the manually delineated terminus trace to ensure that the majority of the terminus is captured by the latter. The observation is excluded if the length of the extrapolation exceeds the length of the delineated terminus.

These processing steps are conducted for the upper and lower boundary separately and terminus delineations are saved once completed.

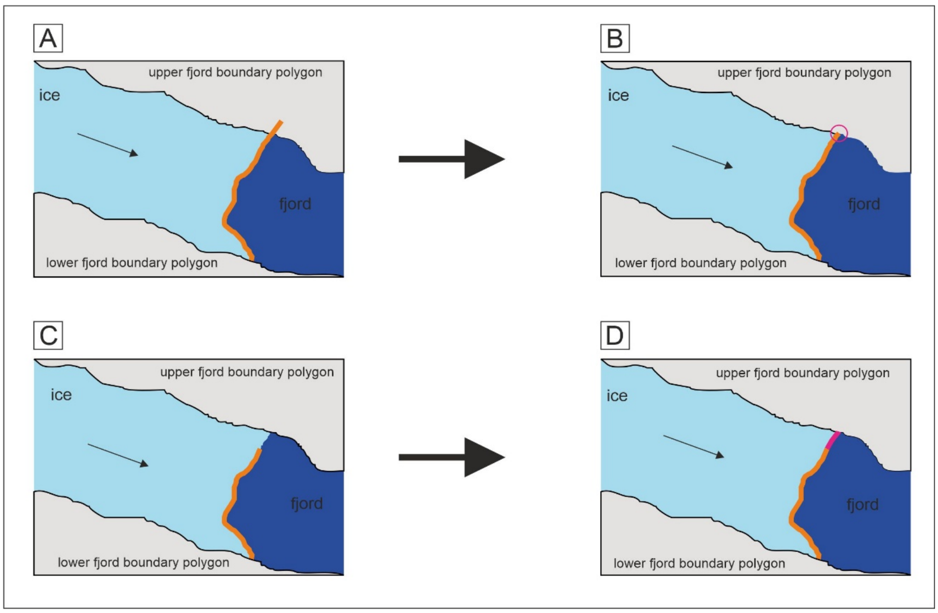

Figure 5 | Sketch of trace cropping/extrapolation

Sketch showing how terminus delineations are cropped or extrapolated. A) If terminus delineation is drawn across the fjord boundary, terminus delineation is cropped to the intersection with the fjord boundary (B). C) If terminus delineation does not intersect or reach the fjord boundary, the delineation is extrapolated to the nearest point on the fjord boundary from the delineation endpoint (D). Small arrow shows glacier flow direction.

Surface elevation change and ice thickness

Ice surface elevation is estimated for the terminus area at the time of each individual terminus observation based on i) Khan (2017) if surface elevation change data are available for the

https://doi.org/10.5194/essd-2023-411
Preprint. Discussion started: 11 December 2023

Open Access Earth System Science Data Discussions

individual tidewater glacier (hereafter referred to as Khan surface change rate or *K-SCR*), and ii) the elevation difference between the ArcticDEM (Porter et al. 2018) and the AeroDEM (Korsgaard et al., 2016a) divided by the time difference (hereafter referred to as ArcticDEM-AeroDEM surface change rate or AA-*SCR*). A workflow schematic is shown in Figure 6.

If K-SCR data are available and the terminus observation date (TOD) is within the K-SCR time range, the annual mean of the K-SCR within the AOI is calculated. The elevation of the latest ArcticDEM is then adjusted by summing the K-SCR for the time difference between the ArcticDEM and terminus observation date (Figure 6). For terminus observations outside the K-SCR time range, the elevation of the ArticDEM is adjusted by summing the K-SCR for all available dates and adding the AA-SCR multiplied by the time difference between the end of

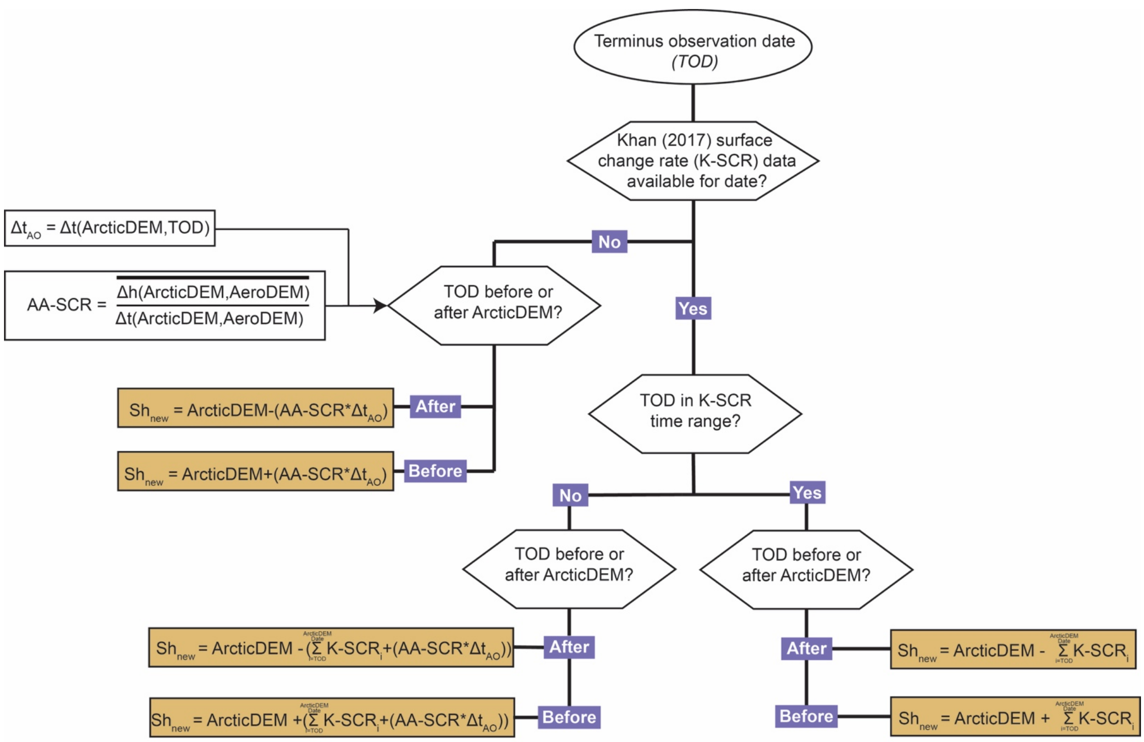

Figure 6 | Process chart for determining surface elevation

The process chart shows how surface elevation for a given terminus observation is determined based on the date of the terminus observation (TOD), the availability of surface elevation change rate data from Khan (2017) referred to as K-SCR, and the difference between ArcticDEM and AeroDEM divided by their time difference (AA-SCR).

https://doi.org/10.5194/essd-2023-411
Preprint. Discussion started: 11 December 2023

K-SCR data and the terminus observation. This allows one to account for surface elevation change prior/after the K-SCR time range, assuming that the surface elevation change is linear for that time period (Figure 6).

If no data are available from Khan (2017) for the selected tidewater glacier, the SCR is multiplied by the time difference between terminus observation and the ArcticDEM. The resulting surface change rate is then subtracted from or added to the ArcticDEM based on the date of the terminus observation (added if the terminus observation is earlier than the ArcticDEM). This method assumes linear surface elevation change and does not account for intra- or inter-annual variability, which introduces uncertainties that could influence the frontal ablation calculation.

The ice thickness H for each terminus observation is then calculated as the difference between the adjusted surface elevation from the underlying bedrock topography (Morlighem et al., 2017, 2021). In the subsequent processing step, the volume for each individual terminus observation polygon is calculated by multiplying the area A_P of the polygon with the mean ice thickness H.

Frontal Ablation Calculation

We first calculate the mass for each terminus observation using the previously created 3-D polygon and an ice density of 0.917g/cm^3 (Figure 7). The presence of significant crevassing near the termini of tidewater glaciers means that some portion of the polygon is in fact air rather than ice, so that the effective density of the polygon will be smaller than that of pure ice. We are not aware of a study that estimates such an effective density, but on the basis of papers that have mapped crevasses (e.g. Enderlin and Bartholomaus, 2020; Van Wyk de Vries et al., 2023) we do not expect a substantial difference from the density of pure ice. As such, we proceed with the pure ice density, but we bear in mind that this may be an upper bound. For each timestep, the respective mass is then linearly interpolated to the first of each month, and mass change over the month in Gt/d is then calculated as the difference in the

https://doi.org/10.5194/essd-2023-411
Preprint. Discussion started: 11 December 2023

mass divided by the number of days in the month. The same processing steps are then applied to ice discharge (D) and finally, frontal ablation (F) is calculated as in Eq. 5. With the applied interpolation and averaging, the results can be interpreted as the mean value over the month in question. The final dataset of frontal ablation contains the interpolated as well as the original values of mass change and solid ice discharge. A sketch of the mass change calculation is illustrated in Figure 7.

The processing chain provides the possibility to estimate monthly, three-monthly or annual frontal ablation. Note that the frontal ablation estimate should be considered as an average over the time period. We recommend use of the three-monthly or annual estimates because the monthly estimates are more susceptible to errors in the terminus delineation induced for instance by pixel size of the satellite image or individual delineation error. In the results shown below we present the three-monthly estimates.

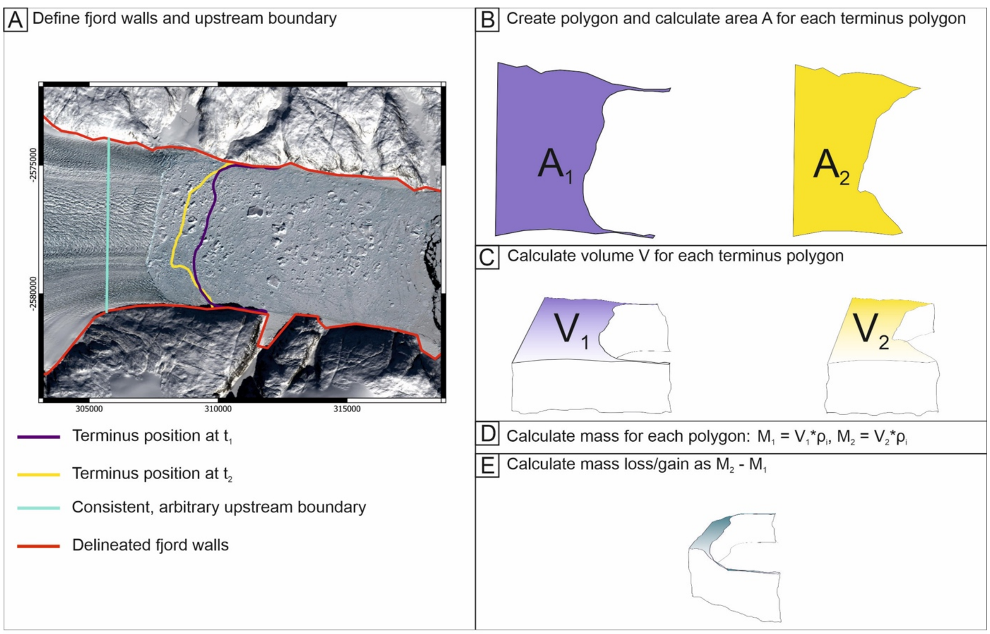

Figure 7 | Sketch of mass loss calculation

A) Example of two consecutive terminus delineations (purple at t_1, yellow at t_2), fjord wall boundaries (red) and upstream boundary (cyan) at Helheim Glacier, SE Greenland, on top of panchromatically sharpened NASA Landsat 9 image from 06/04/2022. B) Created polygons with area A_1 and A_2, corresponding to terminus delineations at times t_1 and t_2. C) Created 3D polygons with volume V_1 and V_2, corresponding to terminus delineations at t_1 and t_2 D) Calculate Mass M_1 and M_2 using $M=V\rho_i$. E) Determine mass change between terminus delineations defined as difference between masses M_1 and M_2 (which in the case shown here is negative).

Uncertainty quantification

The above-described input data products contain glacier- and time-dependent uncertainties, so that errors are introduced to the frontal ablation estimates presented here. To quantify the uncertainty in frontal ablation estimates for each individual tidewater glacier investigated in this study, the uncertainties of the input data products are propagated through the processing chain using error propagation.

Frontal ablation is defined as the difference between solid ice discharge and mass change at the terminus (Eq. 5; Cogley et al., 2011). If the error on solid ice discharge (D) is ΔD, which we take from Mankoff et al. (2020), and the error on terminus mass change (TMC) is ΔTMC, then the uncertainty in frontal ablation ΔF is:

$$\Delta\mathrm{F} = \sqrt{(\Delta D)^2 + (\Delta\mathrm{TMC})^2} \qquad (6)$$

We neglect the uncertainty of ice density (ρ_i; cf. Mankoff et al. (2020)) and calculate TMC as the difference between two volumes separated by a time t_2-t_1 (Figure 7):

$$\mathrm{TMC} = \rho_i \frac{V_2 - V_1}{t_2 - t_1} \qquad (7)$$

To estimate the error on TMC, we neglect uncertainty in the ice density and approximate the difference between the volumes as a cuboid of width W, thickness H and length L (i.e., if the glacier has retreated between t_1 and t_2 then W is the fjord width, H is the ice thickness and L is the retreat length). Neglecting the error on fjord width, we can then estimate the error on V_2-V_1 as

$$\Delta\mathrm{V} = \sqrt{\mathrm{W}^2\mathrm{H}^2\Delta\mathrm{L}^2 + \mathrm{W}^2\mathrm{L}^2\Delta\mathrm{H}^2} \qquad (8)$$

where ΔH = maximum ice thickness error and ΔL = terminus delineation error.

The delineation uncertainty ΔL is based on the satellite that was used to delineate the terminus position. While previous studies suggest relatively small delineation errors, these estimates are for a single operator and only for Landsat 7/8 and Sentinel 1 (Brough et al., 2019; Fahrner

https://doi.org/10.5194/essd-2023-411
Preprint. Discussion started: 11 December 2023

Open Access Earth System Science Data Discussions

et al., 2021). To account for multiple operators and varying satellites, we choose to keep the delineation error constant at 30 meters, which is the average pixel resolution of Landsat satellites (Landsat 4–6-pixel resolution: 60 meters; Landsat 7–8-pixel resolution: 15 meters).

The maximum terminus change is time-averaged over a user defined period (monthly, three-monthly, annually) to conform with the calculation of frontal ablation. Combining Eqs. 7 and 8, we can then determine the uncertainty (ΔTMC) on terminus mass change for each time-averaged step as:

$$\Delta \mathrm{TMC} = \frac{\rho_i}{t_2 - t_1} \Delta V \qquad (9)$$

Where t_2-t_1 is the time resolution of the frontal ablation dataset (31 days, 90 days, 365 days), chosen as 90 days in our results. Eq. 9 gives uncertainties which change in time, but for simplicity in the results and analysis we take a single value which is the maximum over the analysis period. With the described uncertainty of terminus mass change and discharge estimates (Mankoff et al., 2020), we can ultimately calculate the maximum uncertainty of frontal ablation using Eq. 6.

Results

Results for all investigated tidewater glaciers with observation-based bed geometries can be found in Figures S2 – 53. As an example of the impact of terminus change on frontal ablation time series, the frontal ablation and solid ice discharge time series for Helheim Glacier, SE Greenland are shown for the period 1987 – 2020 (Figure 8). The temporal resolution and coverage of the data shown for Helheim Glacier is representative of all study sites.

In accordance with an increase in ice velocity and terminus retreat, frontal ablation for Helheim glacier in SE Greenland shows a sharp rise starting in 2004/05 (Figure 8A-C). These results are consistent with a large-scale retreat during this time frame as determined by previous

https://doi.org/10.5194/essd-2023-411
Preprint. Discussion started: 11 December 2023

Open Access Earth System Science Data Discussions

studies (e.g. Howat et al., 2005, 2008). The results further show that relatively high frontal ablation rates remain present over the following decade and are accompanied by sustained yet seasonally varying terminus retreat, decreasing ice velocities and relatively stable ice discharge (Figure 8B - D). To highlight the influence of terminus position change on frontal ablation, colors shown in Figure 8D correspond directly to the terminus positions used in calculating frontal ablation (Figure 8E). It is seen that while the ice discharge has limited seasonal variability (Fig. 8C), periods where there is seasonal advance and retreat of the terminus (Fig. 8B) result in seasonal variability in frontal ablation (Fig. 8C). The sustained period of retreat from 2000-2005 is driven by frontal ablation values that frequently exceed the ice discharge and reach up to 50% above the ice discharge for three-month periods. It is apparent from Figure 8C that frontal ablation estimates that take terminus change into account show a higher variability than those derived from ice discharge alone (Mankoff et al., 2020).

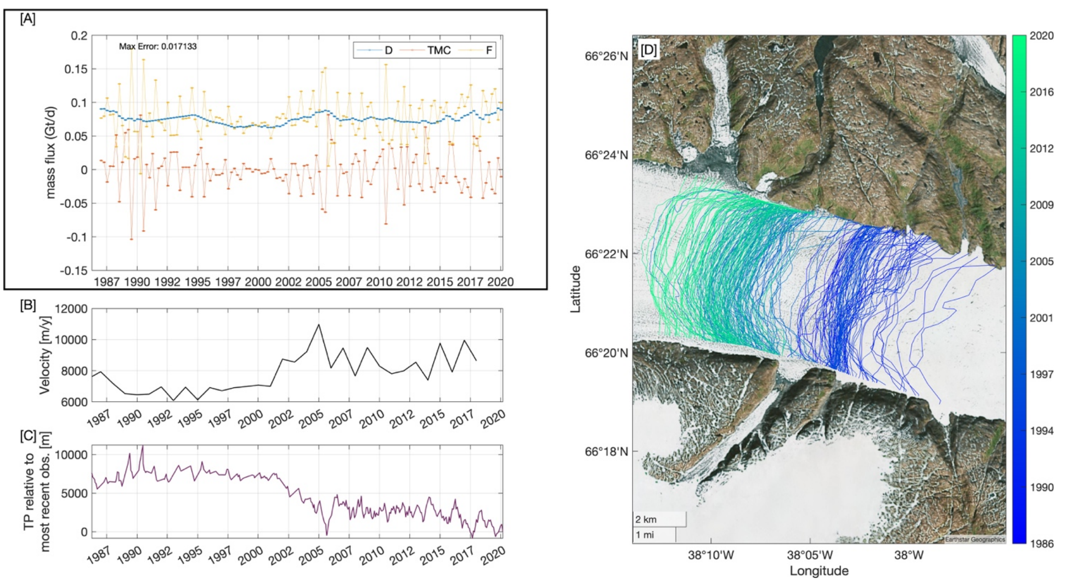

Figure 8 | Example of output data

Example of output data for Helheim Glacier, SE Greenland shown in A) with three-monthly frontal ablation estimates shown in yellow, and discharge (blue) and terminus associated mass change (TMC, red) shown for comparison. Maximum error is also shown (for details see supplementary). B) Annual flow velocity in m/yr from NASA ITS_LIVE data B) Terminus position (TP) relative to most recent observation along the centerline. Panels B) and C) are only shown for validation purposes and are not part of the dataset. D) Terminus positions used to calculate frontal ablation estimates colour coded by date.

https://doi.org/10.5194/essd-2023-411
Preprint. Discussion started: 11 December 2023

Open Access Earth System Science Data Discussions

Figure 9 shows the annual average frontal ablation for a period where terminus observations are available for all tidewater glaciers (1987 – 2018). Helheim Glacier, Kangerlussuaq Glacier and Sermeq Kujalleq (Jakobshavn Isbræ) contribute the most to the total frontal ablation of the investigated glaciers (Figure 9, Table S2). However, seven additional tidewater glaciers around the GrIS show comparatively large frontal ablation values for the same time period (namely: Kangiata Nunaata Sermia (5.65 Gt/yr), Nansen Glacier (6.35 Gt/yr), Sermeq Kujalleq in the Central West (7.68 Gt/yr), Sermeq Kujalleq (Store Glacier; 9.14 Gt/yr), Daugaard-Jensen Glacier (9.48 Gt/yr), Kangiliup Sermia (Rink Isbræ; 12.78 Gt/yr), and Tuttulikassaap Sermia (13.35 Gt/yr). The majority of the studied tidewater glaciers (31 glaciers or ~63 %)

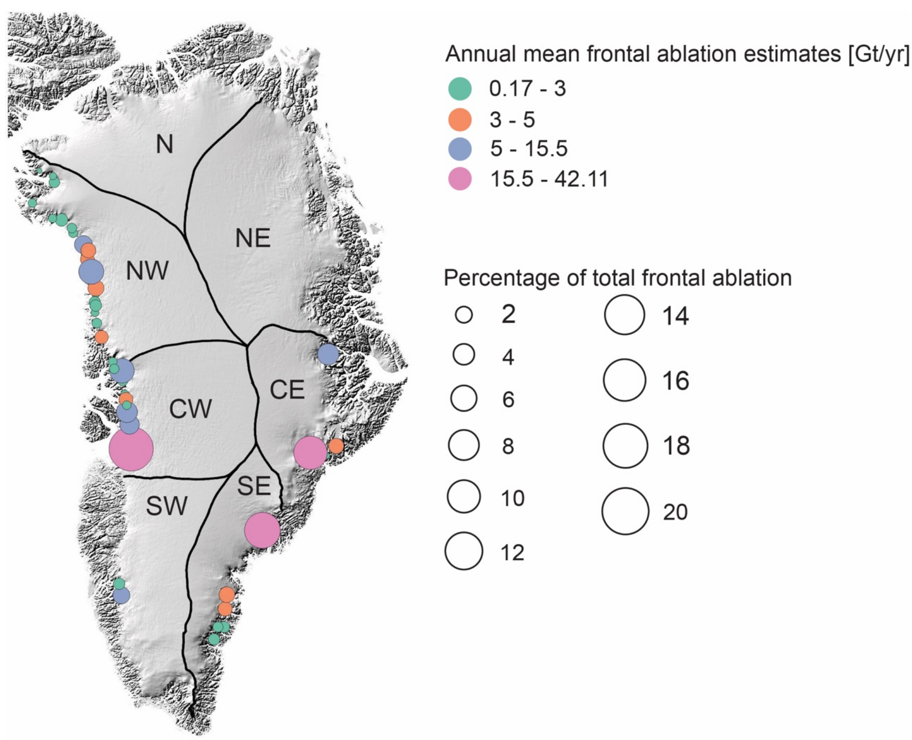

Figure 9 | Overview of total frontal ablation 1987-2015

Overview of total frontal ablation (sum of three-monthly averages) for all tidewater glaciers investigated in this study for the period 1987-2015 (period when terminus observations are available for all tidewater glaciers). Colors show the mean annual frontal ablation estimate for each tidewater glacier; Circle size indicates contribution of mean frontal ablation to the total frontal ablation of all tidewater glaciers. The basemap is taken from BedMachine v4 (Morlighem et al., 2017, 2021), with lines indicating drainage basins (Mouginot et al., 2019)

https://doi.org/10.5194/essd-2023-411
Preprint. Discussion started: 11 December 2023

have frontal ablation values smaller than 3 Gt/yr while eight glaciers have mean annual frontal ablation values between 3 and 5 Gt/yr (Table S2).

The processing chain presented here provides a novel way to estimate frontal ablation rates over long temporal scales, while also taking changes in terminus position into account. The results show that over seasonal timescales (e.g. 3 months), frontal ablation rates that take terminus position change into account can be significantly higher than estimates from ice discharge alone, thereby highlighting the importance of including terminus variability at these timescales. A recent study calculated decadal mean frontal ablation estimates for essentially all glaciers in Greenland for the period 2000-2010 and 2010-2020 (Kochtitzky et al., 2023). In comparison our study focuses on fewer glaciers but at higher temporal resolution. When comparing glaciers that are included in both studies, and calculating decadal mean values from our dataset, we find that for the period 2000-2010 the majority of our estimates (>80%) are within the uncertainty boundaries of Kochtitzky et al. (2023; Figure 10; Table S 3). Agreement is reduced for the period 2010-2020, with roughly half of our frontal ablation estimates (~51%) agreeing with Kochtitzky et al. (2023) within uncertainty, however we find higher estimates for ~40% (17 glaciers) and lower estimates for ~9% (4 glaciers). For all tidewater glaciers investigated in this study, we estimate total decadal frontal ablation to be 217.1 ± 68.6 Gt/yr for the period 2000-2010, and 245.5 ± 68.6 Gt/yr for the period 2010-2020, which agrees within uncertainty with the total over same glaciers in Kochtitzky et al. (2023; Table S3). It should be noted that our study has a very different temporal resolution to Kochtitzky et al. (2023) – three-monthly here versus decadal in their study – and that when summing our three-monthly values to obtain decadal means we cautiously assumed that the errors are fully systematic, which explains the larger uncertainty bounds on our decadal values quoted above.

https://doi.org/10.5194/essd-2023-411
Preprint. Discussion started: 11 December 2023

Open Access Earth System Science Data Discussions

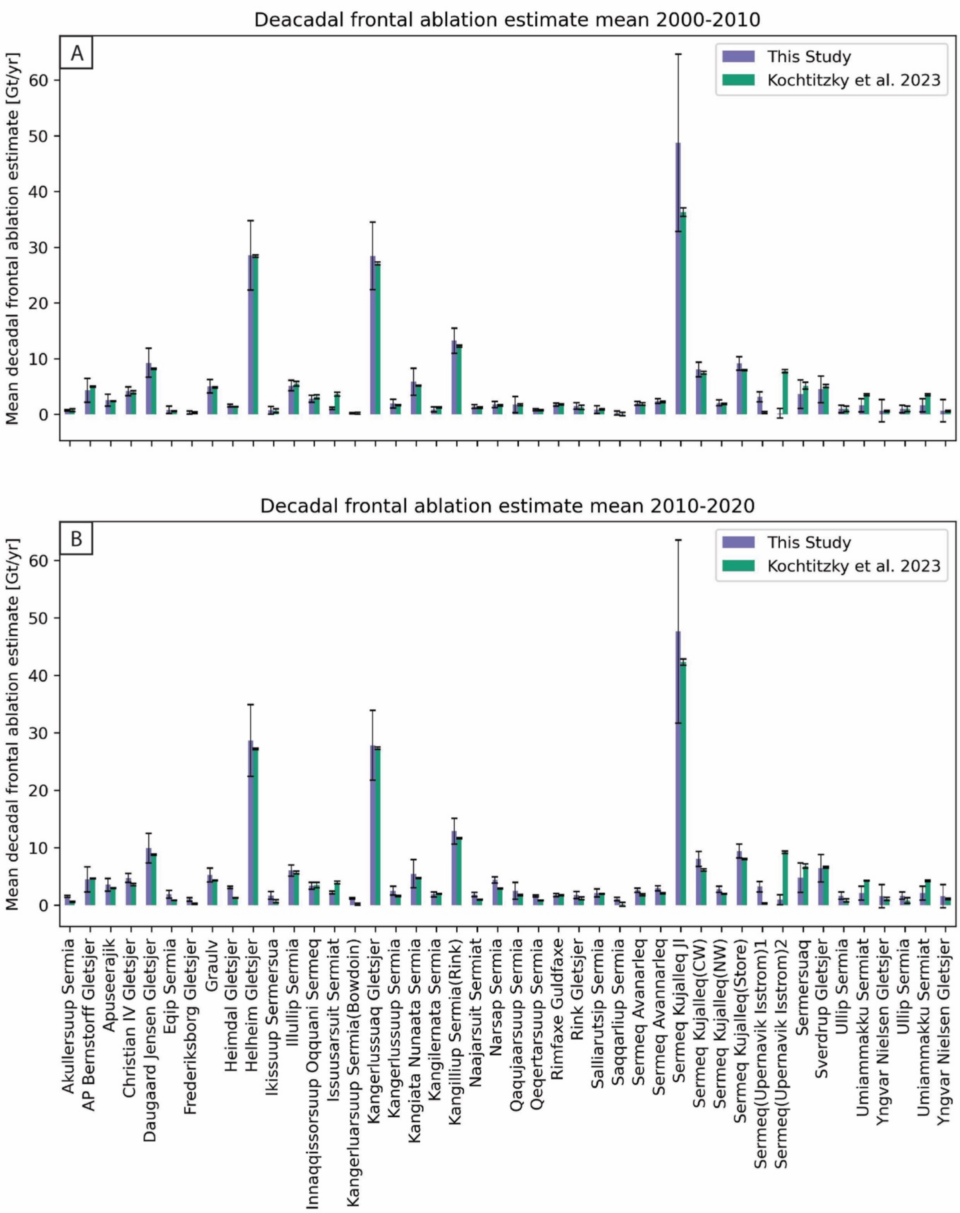

Figure 10 | Comparison of results from Kochtitzky et al. (2023) and this study

A) Comparison of decadal mean frontal ablation estimates presented in this study to results from Kochtitzky et al. (2023) for the period 2000-2010 with uncertainties. B) Comparison of decadal mean frontal ablation estimates presented in this study to results from Kochtitzky et al. (2023) for the period 2010-2020 with uncertainties.

394

https://doi.org/10.5194/essd-2023-411
Preprint. Discussion started: 11 December 2023

The differences in decadal frontal ablation values between our study and Kochtitzky et al. (2023) may result from the higher temporal resolution of terminus delineations used in this study; values which have to be summed to get decadal means in order to do the comparison. However, a degree of the difference also arises from the ice discharge – for example at Sermeq Kujalleq (Jakobshavn Isbræ), the 2000-2010 mean ice discharge used in this study is 41.8 Gt/yr (Mankoff et al., 2020) compared to 34.0 Gt/yr in Kochtitzky et al. (2023).

This study aims to provide the basis for further investigation of the influence of ocean forcing on tidewater glacier termini, and to enable the generation of improved parameterizations of ocean forcing for numerical ice sheet models. Importantly, the processing chain can easily be modified to apply to any tidewater glacier, provided that the following data are available:

1) Terminus positions bracketing the time period of interest.
   To determine frontal ablation on inter-annual or smaller timescales, we suggest providing as many terminus delineations that have been created by a single operator as possible to reduce spatial variability between observations.
2) A satellite image for manual delineation of fjord and upstream boundaries
3) Bedrock topography and surface elevation data to calculate ice thickness for the individual terminus positions.

Conclusion

The dataset presented here provides three-monthly frontal ablation estimates for 49 tidewater glaciers based on terminus position changes for each glacier, yet the processing chain can easily be used to investigate frontal ablation at different temporal resolutions for example monthly or annual. The dataset offers opportunities for the community to investigate the drivers of mass loss at tidewater glaciers in Greenland and provides the basis to improve current parameterizations of climate forcing in model hindcasting and projections.

The results show that over seasonal or shorter time periods, formal ablation estimates that include terminus position change can differ significantly (up to ~50%) from those that are

https://doi.org/10.5194/essd-2023-411
Preprint. Discussion started: 11 December 2023

derived from ice discharge alone. This illuminates the seasonal variability in frontal ablation at tidewater glaciers and may shed light on the processes that drive mass loss at tidewater glacier termini.

A brief example analysis of the dataset shows, that Sermeq Kujalleq (Jakobshavn Isbræ), Kangerlussuaq glacier and Helheim glacier dominate annual frontal ablation estimates in Greenland. However, we also find eight tidewater glaciers with comparatively high frontal ablation estimates, which highlights that large mass loss is not necessarily confined to the most dynamic tidewater glaciers. The results presented here are in agreement with a previously published dataset (Kochtitzky et al., 2023) when considering the sum of frontal ablation over all 49 glaciers, but differences exist at individual glaciers. However, the focus of this study is on fewer glaciers at seasonal time resolution, making the dataset suitable for investigating terminus mass loss processes.

We also hope that the processing chain will be a useful tool to quantify frontal ablation for any glacier, as it is computationally inexpensive and can be adjusted easily. We further plan to develop the processing chain into a standalone tool that can be hosted on GHub, thereby making it fully open source to the community.

Glossary

Solid Ice discharge [Gt/yr]: Volume of ice flowing through a defined transect (or gate) upstream of the terminus.

Ice velocity [m/yr]: Flow velocity of the ice as determined from NASA Landsat satellite imagery.

Surface elevation change rate [m/yr]: Change in surface elevation over time.

Terminus Mass change [km^3/timestep]: Change of mass, which is calculated as near-terminus volume change times ice density (917 kg/m^3).

Frontal ablation [Gt/d]: Total loss of ice at the glacier front, which comprises iceberg calving, submarine melting and subaerial melting (Truffer and Motyka, 2016). We define frontal ablation as the difference between terminus mass change and solid ice discharge, with the sign of mass change being dependent on the terminus configuration (advance = positive, stable =0, retreat=negative).

https://doi.org/10.5194/essd-2023-411
Preprint. Discussion started: 11 December 2023

Author Contributions

DF and all co-authors conceived the study. DF created the processing chain, pre-processed the data, conducted all data analysis, figure production, and led the manuscript writing. All co-authors provided conceptual and technical advice.

Competing financial interests

The authors declare no competing financial interests.

Corresponding Author

Correspondence and request for material should be addressed to dfahrner@uoregon.edu

Data Availability

The complete dataset with uncertainties can be found at https://zenodo.org/records/10278419(Fahrner et al., 2023a).

Greenland Ice Sheet drainage basins can be found at https://doi.org/10.7280/D1WT11 (Mouginot and Rignot, 2019). Tidewater glacier terminus positions from the TermPicks dataset can be found at https://zenodo.org/records/5117931 (Goliber and Black, 2021). ArcticDEM data can be accessed at https://doi.org/10.7910/DVN/OHHUKH (Porter et al., 2018). AeroDEM data can be accessed at https://doi.org/10.7289/v56q1v72 (Korsgaard et al., 2016a). Bedmachine v4 bedrock topography data can be accessed at https://doi.org/10.5067/VLJ5YXKCNGXO (Morlighem et al., 2021). Solid Ice discharge data can be found at https://doi.org/10.22008/promice/data/ice_discharge/d/v02 (Mankoff et al., 2020). Surface elevation change rates can be found at https://doi.org/10.22008/FK2/GQJJEA (Khan, 2017).

The processing chain to produce this dataset including example data and a tutorial is available at https://zenodo.org/records/10278429 (Fahrner et al., 2023b). The processing chain will also be made available on GHub, so that it can be run as a standalone tool.

References

Benn, D.I., Cowton, T., Todd, J. and Luckman, A., (2017) Glacier calving in Greenland. *Current Climate Change Reports*, 34, pp.282–290.

Brough, S., Carr, J.R., Ross, N. and Lea, J.M., (2019) Exceptional retreat of Kangerlussuaq Glacier, east Greenland, between 2016 and 2018. *Frontiers in Earth Science*, 7123.

Bunce, C., Nienow, P., Sole, A., Cowton, T. and Davison, B., (2021) Influence of glacier runoff and near-terminus subglacial hydrology on frontal ablation at a large Greenlandic tidewater glacier. *Journal of Glaciology*, [online] 67262, pp.343–352. Available at: https://www.cambridge.org/core/article/influence-of-glacier-runoff-and-nearterminus-subglacial-hydrology-on-frontal-ablation-at-a-large-greenlandic-tidewater-

https://doi.org/10.5194/essd-2023-411
Preprint. Discussion started: 11 December 2023

glacier/39F8B5452292F955FA58CA6DE3921544.

Cogley, J.G., Hock, R., Rasmussen, L.A., Arendt, A.A., Bauder, A., Braithwaite, R.J., Jansson, P., Kaser, G., Möller, M. and Nicholson, L., (2011) Glossary of glacier mass balance and related terms, IHP-VII technical documents in hydrology No. 86, IACS Contribution No. 2. International Hydrological Program. *UNESCO, Paris. doi*, 10, pp.1938–4246.

Cowton, T.R., Sole, A.J., Nienow, P.W., Slater, D.A. and Christoffersen, P., (2018) Linear response of east Greenland's tidewater glaciers to ocean/atmosphere warming. *Proceedings of the National Academy of Sciences*, 11531, pp.7907–7912.

Enderlin, E.M. and Bartholomaus, T.C., (2020) Sharp contrasts in observed and modeled crevasse patterns at Greenland's marine terminating glaciers. *The Cryosphere*, [online] 1411, pp.4121–4133. Available at: https://tc.copernicus.org/articles/14/4121/2020/.

Enderlin, E.M., Hamilton, G.S., O'Neel, S., Bartholomaus, T.C., Morlighem, M. and Holt, J.W., (2016) *An Empirical Approach for Estimating Stress-Coupling Lengths for Marine-Terminating Glaciers* . *Frontiers in Earth Science* , Available at: https://www.frontiersin.org/articles/10.3389/feart.2016.00104.

Enderlin, E.M., Howat, I.M., Jeong, S., Noh, M.-J., Angelen, J.H. and Broeke, M.R., (2014) An improved mass budget for the Greenland ice sheet. *Geophysical Research Letters*, 413, pp.866–872.

Fahrner, D., Lea, J.M., Brough, S., Mair, D.W.F. and Abermann, J., (2021) Linear response of the Greenland ice sheet's tidewater glacier terminus positions to climate. *Journal of Glaciology*, [online] 67262, pp.193–203. Available at: https://www.cambridge.org/core/article/linear-response-of-the-greenland-ice-sheets-tidewater-glacier-terminus-positions-to-climate/6B3723E3A0E94012A1DB9D3E49246AF2.

Fahrner, D., Slater, D., KC, A., Cenedese, C., Sutherland, D.A., Enderlin, E., Jong, F. de, Kjeldsen, K.K., Wood, M., Nienow, P., Nowicki, S. and Wagner, T., (2023a) *Frontal ablation estimates for 49 tidewater glaciers in Greenland*. Available at: https://zenodo.org/records/10278419.

Fahrner, D., Slater, D., KC, A., Cenedese, C., Sutherland, D.A., Enderlin, E., Jong, F. de, Kjeldsen, K.K., Wood, M., Nienow, P., Nowicki, S. and Wagner, T., (2023b) *Tidewater Glacier Frontal Ablation Tool - TG_FACT*. Available at: https://zenodo.org/records/10278429.

Fried, M.J., Catania, G.A., Stearns, L.A., Sutherland, D.A., Bartholomaus, T.C., Shroyer, E. and Nash, J., (2018) Reconciling Drivers of Seasonal Terminus Advance and Retreat at 13 Central West Greenland Tidewater Glaciers. *Journal of Geophysical Research: Earth Surface*, 1237, pp.1590–1607.

Gardner, A.S., Fahnestock, M.A. and Scambos, T.A., (2019) *ITS_LIVE Regional Glacier and Ice Sheet Surface Velocities, National Snow and Ice Data Center*.

Goelzer, H., Nowicki, S., Payne, A., Larour, E., Seroussi, H., Lipscomb, W.H., Gregory, J., Abe-Ouchi, A., Shepherd, A., Simon, E., Agosta, C., Alexander, P., Aschwanden, A., Barthel, A., Calov, R., Chambers, C., Choi, Y., Cuzzone, J., Dumas, C., Edwards, T., Felikson, D., Fettweis, X., Golledge, N.R., Greve, R., Humbert, A., Huybrechts, P., Le clec'h, S., Lee, V., Leguy, G., Little, C., Lowry, D.P., Morlighem, M., Nias, I., Quiquet, A., Rückamp, M., Schlegel, N.-J., Slater, D.A., Smith, R.S., Straneo, F., Tarasov, L., van de Wal, R. and van den Broeke, M., (2020) The future sea-level contribution of the Greenland ice sheet: a multi-model ensemble study of ISMIP6. *The Cryosphere*, [online] 149, pp.3071–3096. Available at: https://tc.copernicus.org/articles/14/3071/2020/.

Goliber, S. and Black, T., (2021) *TermPicks: A century of Greenland glacier terminus data* *for use inmachine learning applications (Version 1)*. Available at: https://zenodo.org/records/5117931.

Greene, C.A., Gwyther, D.E. and Blankenship, D.D., (2017) Antarctic mapping tools for MATLAB. *Computers & Geosciences*, 104, pp.151–157.

Howat, I.M., Joughin, I., Fahnestock, M., Smith, B.E. and Scambos, T.A., (2008) Synchronous retreat and acceleration of southeast Greenland outlet glaciers 2000--06: Ice dynamics and coupling to climate. *Journal of Glaciology*, 54187, pp.646–660.

Howat, I.M., Joughin, I., Tulaczyk, S. and Gogineni, S., (2005) Rapid retreat and acceleration of Helheim Glacier, east Greenland. *Geophysical Research Letters*, [online] 3222. Available at: https://doi.org/10.1029/2005GL024737.

Khan, S.A., (2017) *Greenland Ice Sheet Surface Elevation Change*. Available at: https://doi.org/10.22008/FK2/GQJJEA.

King, M.D., Howat, I.M., Candela, S.G., Noh, M.J., Jeong, S., Noël, B.P.Y., van den Broeke, M.R., Wouters, B. and Negrete, A., (2020) Dynamic ice loss from the Greenland Ice Sheet driven by sustained glacier retreat. *Communications Earth & Environment*, [online] 11, p.1. Available at: https://doi.org/10.1038/s43247-020-0001-2.

Kochtitzky, W., Copland, L., King, M., Hugonnet, R., Jiskoot, H., Morlighem, M., Millan, R., Khan, S.A. and Noël, B., (2023) Closing Greenland's Mass Balance: Frontal Ablation of Every Greenlandic Glacier From 2000 to 2020. *Geophysical Research Letters*, [online] 5017, p.e2023GL104095. Available at: https://doi.org/10.1029/2023GL104095.

Kochtitzky, W., Copland, L., Van Wychen, W., Hugonnet, R., Hock, R., Dowdeswell, J.A., Benham, T., Strozzi, T., Glazovsky, A., Lavrentiev, I., Rounce, D.R., Millan, R., Cook, A., Dalton, A., Jiskoot, H., Cooley, J., Jania, J. and Navarro, F., (2022) The unquantified mass loss of Northern Hemisphere marine-terminating glaciers from 2000–2020. *Nature Communications*, [online] 131, p.5835. Available at: https://doi.org/10.1038/s41467-022-33231-x.

Köhler, A., Nuth, C., Kohler, J., Berthier, E., Weidle, C. and Schweitzer, J., (2016) A 15 year record of frontal glacier ablation rates estimated from seismic data. *Geophysical Research Letters*, [online] 4323, pp.12,112-155,164. Available at: https://doi.org/10.1002/2016GL070589.

Korsgaard, N.J., Nuth, C., Khan, S.A., Kjeldsen, K.K., Bjørk, A.A., Schomacker, A. and Kjær, K.H., (2016a) *Digital Elevation Model and orthophotographs of Greenland based on aerial photographs from 1978-1987 (G150 AERODEM) (NCEI Accession 0145405)*. Available at: https://doi.org/10.7289/v56q1v72.

Korsgaard, N.J., Nuth, C., Khan, S.A., Kjeldsen, K.K., Bjørk, A.A., Schomacker, A. and Kjær, K.H., (2016b) Digital elevation model and orthophotographs of Greenland based on aerial photographs from 1978–1987. *Scientific Data*, [online] 31, p.160032. Available at: https://doi.org/10.1038/sdata.2016.32.

Luckman, A., Benn, D.I., Cottier, F., Bevan, S., Nilsen, F. and Inall, M., (2015) Calving rates at tidewater glaciers vary strongly with ocean temperature. *Nature Communications*, [online] 61, p.8566. Available at: https://doi.org/10.1038/ncomms9566.

Mankoff, K., Solgaard, A. and Larsen, S., (2020) *Greenland Ice Sheet solid ice discharge from 1986 through last month: Discharge*. V89 ed. Available at: https://doi.org/10.22008/promice/data/ice_discharge/d/v02.

McNabb, R.W., Hock, R. and Huss, M., (2015) Variations in Alaska tidewater glacier frontal ablation, 1985–2013. *Journal of Geophysical Research: Earth Surface*, [online] 1201,

https://doi.org/10.5194/essd-2023-411
Preprint. Discussion started: 11 December 2023

pp.120–136. Available at: https://doi.org/10.1002/2014JF003276.

Morlighem, M., Williams, C., Rignot, E., An, L., Arndt, J.E., Bamber, J., Catania, G., Chauché, N., Dowdeswell, J.A., Dorschel, B., Fenty, I., Hogan, K., Howat, I., Hubbard, A., Jakobsson, M., Jordan, T.M., Kjeldsen, K.K., Millan, R., Mayer, L., Mouginot, J., Noël, B., O'Cofaigh, C., Palmer, S.J., Rysgaard, S., Seroussi, H., Siegert, M.J., Slabon, P., Straneo, F., Broeke, M.R. van den, Weinrebe, W., Wood, M. and Zinglersen, K., (2021) *IceBridge BedMachine Greenland, Version 4*. Available at: https://doi.org/10.5067/VLJ5YXKCNGXO.

Morlighem, M., Williams, C.N., Rignot, E., An, L., Arndt, J.E., Bamber, J., Catania, G., Chauché, N., Dowdeswell, J.A., Dorschel, B. and others, (2017) BedMachine v3: Complete bed topography and ocean bathymetry mapping of Greenland from multibeam echo sounding combined with mass conservation. *Geophysical research letters*, 4421.

Mouginot, J. and Rignot, E., (2019) *Glacier catchments/basins for the Greenland Ice Sheet [Dataset]*. Available at: https://doi.org/10.7280/D1WT11.

Mouginot, J., Rignot, E., Bjørk, A.A., van den Broeke, M., Millan, R., Morlighem, M., Noël, B., Scheuchl, B. and Wood, M., (2019) Forty-six years of Greenland Ice Sheet mass balance from 1972 to 2018. *Proceedings of the National Academy of Sciences*, [online] 11619, pp.9239 LP – 9244. Available at: http://www.pnas.org/content/116/19/9239.abstract.

Murray, T., Scharrer, K., Selmes, N., Booth, A.D., James, T.D., Bevan, S.L., Bradley, J., Cook, S., Llana, L.C., Drocourt, Y. and others, (2015) Extensive retreat of Greenland tidewater glaciers, 2000--2010. *Arctic, Antarctic, and alpine research*, 473, pp.427–447.

Osmanoğlu, B., Braun, M., Hock, R. and Navarro, F.J., (2013) Surface velocity and ice discharge of the ice cap on King George Island, Antarctica. *Annals of Glaciology*, [online] 5463, pp.111–119. Available at: https://www.cambridge.org/core/article/surface-velocity-and-ice-discharge-of-the-ice-cap-on-king-george-island-antarctica/62E511405ADD31A43FF52CDBC727A9D0.

Porter, C., Morin, P., Howat, I., Noh, M.-J., Bates, B., Peterman, K., Keesey, S., Schlenk, M., Gardiner, J., Tomko, K., Willis, M., Kelleher, C., Cloutier, M., Husby, E., Foga, S., Nakamura, H., Platson, M., Wethington Jr., M., Williamson, C., Bauer, G., Enos, J., Arnold, G., Kramer, W., Becker, P., Doshi, A., D'Souza, C., Cummens, P., Laurier, F. and Bojesen, M.A.-N.S.F.A.-N.S.F., (2018) *ArcticDEM*. V1 ed. Available at: https://doi.org/10.7910/DVN/OHHUKH.

Rignot, E. and Kanagaratnam, P., (2006) Changes in the velocity structure of the Greenland Ice Sheet. *Science*, 3115763, pp.986–990.

Shepherd, A., Ivins, E., Rignot, E., Smith, B., van den Broeke, M., Velicogna, I., Whitehouse, P., Briggs, K., Joughin, I., Krinner, G., Nowicki, S., Payne, T., Scambos, T., Schlegel, N., A, G., Agosta, C., Ahlstrøm, A., Babonis, G., Barletta, V.R., Bjørk, A.A., Blazquez, A., Bonin, J., Colgan, W., Csatho, B., Cullather, R., Engdahl, M.E., Felikson, D., Fettweis, X., Forsberg, R., Hogg, A.E., Gallee, H., Gardner, A., Gilbert, L., Gourmelen, N., Groh, A., Gunter, B., Hanna, E., Harig, C., Helm, V., Horvath, A., Horwath, M., Khan, S., Kjeldsen, K.K., Konrad, H., Langen, P.L., Lecavalier, B., Loomis, B., Luthcke, S., McMillan, M., Melini, D., Mernild, S., Mohajerani, Y., Moore, P., Mottram, R., Mouginot, J., Moyano, G., Muir, A., Nagler, T., Nield, G., Nilsson, J., Noël, B., Otosaka, I., Pattle, M.E., Peltier, W.R., Pie, N., Rietbroek, R., Rott, H., Sandberg Sørensen, L., Sasgen, I., Save, H., Scheuchl, B., Schrama, E., Schröder, L., Seo, K.-W., Simonsen, S.B., Slater, T., Spada, G., Sutterley, T., Talpe, M., Tarasov, L., van de Berg, W.J., van der Wal, W., van Wessem, M., Vishwakarma, B.D., Wiese, D., Wilton, D., Wagner, T., Wouters, B., Wuite, J. and Team, T.I., (2020) Mass balance of the Greenland Ice Sheet from 1992 to 2018. *Nature*, [online] 5797798, pp.233–239. Available at: https://doi.org/10.1038/s41586-019-1855-2.

https://doi.org/10.5194/essd-2023-411
Preprint. Discussion started: 11 December 2023

Slater, D.A., Straneo, F., Felikson, D., Little, C.M., Goelzer, H., Fettweis, X. and Holte, J., (2019) Estimating Greenland tidewater glacier retreat driven by submarine melting. *The Cryosphere*, 139, pp.2489–2509.

Truffer, M. and Motyka, R.J., (2016) Where glaciers meet water: Subaqueous melt and its relevance to glaciers in various settings. *Reviews of Geophysics*, [online] 541, pp.220–239. Available at: https://doi.org/10.1002/2015RG000494.

Wagner, T.J.W., Straneo, F., Richards, C.G., Slater, D.A., Stevens, L.A., Das, S.B. and Singh, H., (2019) Large spatial variations in the flux balance along the front of a Greenland tidewater glacier. *The Cryosphere*, [online] 133, pp.911–925. Available at: https://tc.copernicus.org/articles/13/911/2019/.

Wood, M., Rignot, E., Fenty, I., An, L., Bjørk, A., van den Broeke, M., Cai, C., Kane, E., Menemenlis, D., Millan, R., Morlighem, M., Mouginot, J., Noël, B., Scheuchl, B., Velicogna, I., Willis, J.K. and Hong, Z., (2021) Ocean forcing drives glacier retreat in Greenland. *Science Advances*, [online] 71, p.eaba7282. Available at: https://doi.org/10.1126/sciadv.aba7282.

Wychen, W. Van, Burgess, D., Kochtitzky, W., Nikolic, N., Copland, L. and Gray, L., (2020) RADARSAT-2 Derived Glacier Velocities and Dynamic Discharge Estimates for the Canadian High Arctic: 2015–2020. *Canadian Journal of Remote Sensing*, [online] 466, pp.695–714. Available at: https://doi.org/10.1080/07038992.2020.1859359.

Van Wyk de Vries, M., Lea, J.M. and Ashmore, D.W., (2023) Crevasse density, orientation and temporal variability at Narsap Sermia, Greenland. *Journal of Glaciology*, [online] pp.1–13. Available at: https://www.cambridge.org/core/article/crevasse-density-orientation-and-temporal-variability-at-narsap-sermia-greenland/0B88B733EEB4C04C8C7AA9466FCB99A6.